International Journal of Minerals, Metallurgy and Materials
Accepted manuscript, https://doi.org/10.1007/s12613-020-2205-y

The activity coefficient of nickel oxide in SiO_2 saturated MnO-SiO_2 slag and Al_2O_3 saturated MnO-SiO_2-Al_2O_3 slag at 1623K

Guo-xing Ren[1,2)], Song-wen Xiao[2)], Cai-bin Liao[2)], and Zhi-hong Liu[1)]

1) School of Metallurgy and Environment, Central South University, Changsha 410083, China

2) Changsha Research Institute of Mining & Metallurgy CO., Ltd, Changsha 410012, China

The following are the information of all co-authors of this paper:

Guo-xing Ren, [1)] School of Metallurgy and Environment, Central South University, Changsha, China; [2)] Changsha Research Institute of Mining & Metallurgy CO., Ltd., Changsha, China
Email: rgxrgx@126.com

Song-wen Xiao, Changsha Research Institute of Mining & Metallurgy CO., Ltd., Changsha, China,
Email: swinxiao@126.com

Cai-bin Liao, Changsha Research Institute of Mining & Metallurgy CO., Ltd., Changsha, China,
Email: 15551789509@163.com

Zhi-hong Liu, School of Metallurgy and Environment, Central South University, Changsha, China,
Email: zhliu@csu.edu.cn; Tel: +8613873117863

Corresponding author: Zhi-hong Liu, E-mail: zhliu@csu.edu.cn

Co-corresponding author: Song-wen Xiao, E-mail: swinxiao@126.com

Abstract: As a part of the fundamental study related to the reduction smelting of both spent lithium-ion batteries and polymetallic sea nodules based on MnO-SiO_2-based slags, the activity coefficient of nickel oxide in SiO_2 saturated MnO-SiO_2 slag and Al_2O_3 saturated MnO-SiO_2-Al_2O_3 slag at 1623 K was investigated with controlled oxygen partial pressure of 10^{-7}, 10^{-6}, and 10^{-5} Pa. The results show that the solubility of nickel oxide in the slags increased with increasing the oxygen partial pressure. The nickel in both MnO-SiO_2 slag and MnO-SiO_2-Al_2O_3 slag existed as

NiO under experimental conditions. The addition of Al_2O_3 in the MnO-SiO_2 slag decreased the dissolution of Ni in the slag, and increased the activity coefficient of NiO. Furthermore, the activity coefficient of NiO, referred to solid NiO, can be calculated as:

γ_{NiO}=8.58(wt% NiO in slag) + 3.18 (SiO_2 saturated MnO-SiO_2 slag, 1623 K);

γ_{NiO}=11.06(wt% NiO in slag) + 4.07 (Al_2O_3 saturated MnO-SiO_2-Al_2O_3 slag, 1623 K).

Key: nickel; equilibrium; MnO-SiO_2 slag; MnO-SiO_2-Al_2O_3 slag; activity coefficient

1. Introduction

Social and economic development, especially the electrification of vehicles, will inevitably lead to an enormous increase in nickel demand [1-5]. China, as the world's biggest lithium-ion batteries (LIBs) producer, is seriously short of nickel resources, and needs to import plenty of nickel resources from Indonesia and Philippines [2]. At the same time, Indonesia, one of the world's largest exporters of nickel ore, has banned the export of unprocessed nickel ore as an effort to develop its domestic smelting industry [2]. Hence, to utilize alternative nickel resources for China has become a realistic and urgent issue.

One such alternate resource, of course, is end-of-use LIBs which consume about 600 thousand tons of nickel per year [3]. They are typically constituted by a metal shell, a cathode, an anode, organic electrolyte, and a polymer diaphragm. The anode is a metallic copper foil coated with graphite using polyvinylidene fluoride (PVDF) as a binder, while the cathode is a metallic aluminum foil covered with lithium-transition-metal-oxide powders such as $LiCoO_2$, $LiMn_2O_4$, $LiNiO_2$, and $LiCo_xMn_yNi_zO_2$ [1]. The typical elemental composition of LIBs is presented in Table 1. The other potential alternative resource for nickel could be polymetallic sea nodules, which is found at a depth of 3000-5000 meters in the ocean bed, and also called as manganese nodules due

to their high content of manganese [6-14]. Besides manganese, polymetallic sea nodules also contain plenty of nickel, cobalt, copper, iron, and silicon, as shown in Table 1. According to the report by Das [14], nickel availability in polymetallic sea nodules is nearly five times higher than that in land-based mineral resources. Unlike LIBs, nearly all elements in the polymetallic sea nodules are presented in the form of oxides.

Table 1. Main elemental composition of lithium-ion batteries [5, 15]

Constituents	Content/ wt%	Constituents	Content/ wt%
Ni	1-10	Al	10-33
Cu	8-16	Mn	0-21
Co	5-20	C	10-17

Table 2. Typical composition of polymetallic sea nodules [8, 11]

Constituents	Content/ wt%	Constituents	Content/ wt%
Ni	0.90-1.36	Zn	0.08-0.15
Cu	0.66-1.17	Mo	0.04-0.06
Co	0.073-0.37	SiO_2	12.64-19.22
Fe	6.20-16.99	Al_2O_3	3.79-5.79
Mn	20.03-31.23	CaO	2.27-2.97

To date, many methods have been developed to extract valuable metals (Ni, Co and Cu) from polymetallic sea nodules, such as high-pressure sulfuric acid leaching, reduction-ammonia leaching, reduction roasting-ammonia leaching, reduction smelting-sulfurization (alloy-to-matte conversion)-hydrometallurgy and reduction smelting-hydrometallurgy combinatorial processes. Among them, the reduction smelting-hydrometallurgy combinatorial process is more feasible in

industry due to its less generation of hazardous leaching residue containing heavy metals, and higher productivity [6-14]. For this process, the nodules are first dried, and then smelt at 1350-1450°C without adding any flux. During smelting, the oxides of Ni, Co, Cu and Fe contained in nodules are reduced by adding cokes as reducing agents, producing a Fe-Co-Cu-Ni alloy, while silica and manganese oxides are enriched into a $MnO\text{-}SiO_2$ slag. The obtained slag is nearly silica saturated (sat.) due to its higher SiO_2 content. After smelting, the obtained Fe-Ni-Cu-Co alloy can be further processed to recover nickel by hydrometallurgical methods including leaching and solvent extraction.

Although spent LIBs differ from polymetallic sea nodules in the form and the content of main elements, both they contain Ni, Co, Cu, and Mn. Thus, a reduction smelting-hydrometallurgy combinatorial process has also been reported to extract valuable metals from spent LIBs [4, 5, 15-17]. During this process, the metallic aluminum foil, graphite anode, and organic materials such as electrolyte and separator are oxidized and used as reducing agents. The oxides of nickel and cobalt contained in cathode materials are reduced and then enriched into an alloy phase together with metallic Cu foil at smelting temperatures of 1300°C -1500°C, while the oxides of manganese and lithium contained in cathode materials are enriched into a $MnO\text{-}SiO_2\text{-}Al_2O_3$ slag phase along with silica flux and alumina generated from the oxidation of metallic Al foil. Generally speaking, the slag obtained from the smelting of spent LIBs is alumina saturated due to the very high content of Al in batteries.

As described above, a smelting-reduction technology based on $MnO\text{-}SiO_2\text{-}(Al_2O_3)$ slag system, as a universal method, can recover nickel from both spent LIBs and polymetallic sea nodules. During the smelting, in order to maximize the recovery of nickel, knowledge on the

activity coefficient of nickel oxide in SiO_2 saturated $MnO\text{-}SiO_2$ and Al_2O_3 saturated $MnO\text{-}SiO_2\text{-}Al_2O_3$ slag is necessary.

Unfortunately, up to now, most information obtained on the activity coefficient of nickel oxide in slag focus on the $FeO_x\text{-}SiO_2$-based slag (fayalite slag) or FeO-CaO-based slag (calcium ferrite slag) which is commonly utilized in the metallurgical processes of traditional minerals. For example, Grimsey measured nickel solubility in SiO_2-saturated $FeO_x\text{-}SiO_2$ slags equilibrated with liquid Ni-Au-Fe alloys at 1523 K and 1623 K under oxygen partial pressures between 10^{-9} atm to 10^{-7} atm [18]. Reddy and Acholonu determined nickel solubility in Al_2O_3-saturated $FeO_x\text{-}SiO_2\text{-}Al_2O_3$ slags equilibrated with Cu-Ni alloys at 1573 K and oxygen partial pressures in the range of 10^{-10} to 10^{-8} atm [19]. They found that adding Al_2O_3 to the iron silicate slag increases the solubility of nickel. Henao *et al*. studied the activity coefficients of NiO in FeO_x-CaO-MgO slags at temperature of 1773 K by equilibrating with the slags with Ni-S melt and under controlled oxygen partial pressures in a range between 5.1×10^{-3} Pa and 1.6 Pa [20]. They found that the values of activity coefficient of NiO (relative to the pure solid NiO) are in the range of 2.7-5.4, which agrees well with the results reported by Takeda *et al*. [21].

Many works have also been conducted to investigate the activity coefficient of NiO in MgO-saturated $FeO_x\text{-}MgO\text{-}SiO_2$ based slag which is widely used for ferronickel smelting process [20, 22-24]. Their results show that the activity coefficient of NiO referred to solid NiO presents values ranging from 2 to 6. Henao *et al*. [20] also determined the activity coefficient of NiO in the $FeO_x\text{-}MgO\text{-}SiO_2$ slag with low S content and reported the values of activity coefficient of NiO, referred to solid NiO, are in the range of 3.1 to 8.8. ~~In addition,~~ Pagador *et al.* [13] and Henao *et al.* [14] also studied the effect of adding Al_2O_3 and CaO into the $FeO_x\text{-}MgO\text{-}SiO_2$ slag on the

activity coefficient of NiO. They found that both CaO and Al_2O_3 increased the activity coefficient of NiO in the FeO_x-MgO-SiO_2 slag.

Additionally, some works also investigated the activity coefficient of NiO in the CaO-Al_2O_3 based slag which was proposed to apply for the deoxidation process of nickel alloy [25-27]. For instance, Henao *et al*. investigated the activity coefficient of NiO in the CaO-Al_2O_3 slag equilibrated with Ni-S alloy or pure nickel metal [25, 26]. They found that the values of activity coefficient of NiO in CaO-Al_2O_3 slag are larger than those in FeO_x-CaO slag, which is explained by the stronger interaction between CaO and Al_2O_3.

In this study, the activity coefficient of nickel oxide in SiO_2 saturated MnO-SiO_2 and Al_2O_3 saturated MnO-SiO_2-Al_2O_3 slag is determined, aiming at obtaining the fundamental data related to the reduction smelting of both spent lithium-ion batteries and polymetallic sea nodules. The experiments were carried out by equilibrating the slag with a Cu-Ni alloy under a controlled oxygen partial pressure with CO-CO_2 gas mixtures at 1623 K.

2. Experimental

The experimental setup used in this study, as schematically shown in Fig. 1, mainly consists of a vertical furnace and a gas purification system. The furnace was equipped with $MoSi_2$ heating elements and an alumina reaction tube (outer diameter: 80 mm, inner diameter: 74 mm, height: 850 mm). The temperature of the furnace was controlled within ±2 K by a B-type thermocouple (Pt-6wt% Rh/Pt-30wt% Rh) which was placed between the reaction tube and heating element. In addition, the temperature of the samples was monitored within ±2 K by using another B-type thermocouple (Pt-6wt% Rh/Pt-30wt% Rh) which is placed close to the samples. The thermocouple was first calibrated by determining its electromotive force at different temperatures

with a multimeter, and the accuracy was further checked against the melting point of pure copper, yielding values ± 2 K of the accepted melting point (1356 K). CO-CO_2 gas mixtures with a total flow rate regulated at 200 cm^3/min were used to control the oxygen partial pressure inside the tube. The CO and CO_2 gases, respectively, were purified, dewatered and accurately measured by passing a tube furnace containing magnesium chips at 873 K, a silica gel flask, molecular sieve and a mass flow controller before they were mixed. The oxygen partial pressure was calculated according to the reaction (T/ K):

$$CO(g) + 1/2O_2 = CO_2\ (g)$$

$$\Delta G^{\theta} = -280000 + 85.23T \quad \text{J/mol} \qquad (1) \quad [24]$$

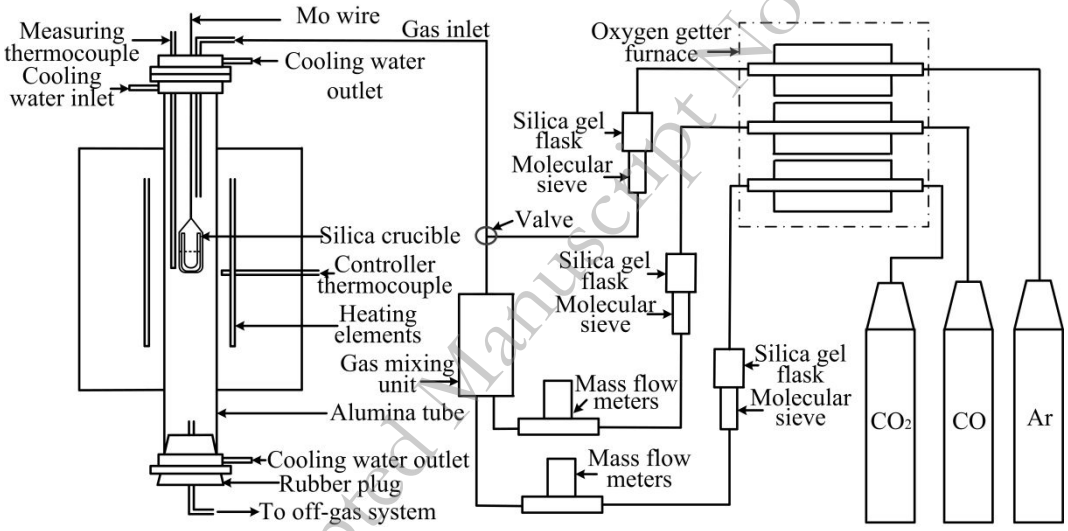

Fig. 1. Schematic diagram of experimental setup.

Copper-nickel master alloys, containing different amounts of nickel, were produced in a tube furnace at 1623 K under argon atmosphere, using Ni powders (99.95wt%, supplied by Sinopharm Chemical Reagent Co., Ltd.) and Cu powders (99.95wt%, supplied by Sinopharm Chemical Reagent Co., Ltd.) as the starting materials. MnO-SiO_2 and MnO-SiO_2-Al_2O_3 master slags were prepared, using SiO_2 (99.99wt%, supplied by Shanghai Aladdin Biochemical Technology Co., Ltd.), Al_2O_3 (99.99wt%, supplied by Sinopharm Chemical Reagent Co., Ltd.) powders, and MnO

powders as the starting materials. MnO powders were obtained by roasting $MnCO_3$ powders (99.99wt%, supplied by Shanghai Aladdin Biochemical Technology Co., Ltd.) at 973 K under an argon atmosphere.

High pure silica and alumina crucibles were used for the MnO-SiO_2 slag and MnO-SiO_2-Al_2O_3 slag experiments, respectively. Before the experiments, the reaction tube was firstly washed with purified argon gas, and then the crucible contained 1.5 g alloy with different content of Ni and 3 g slag (49.66wt% MnO-50.34wt% SiO_2 slag or 30.22wt% MnO-34.58wt% SiO_2-35.20wt% Al_2O_3 slag) were introduced into the hot zone of the furnace at 1623 K. Next, argon flow was stopped and the mixture of CO and CO_2 was immediately switched into the furnace. After the equilibration was established, the samples were rapidly quenched by falling into the cold water. Solidified slags were analyzed for Ni, Cu, Mn, SiO_2 and Al_2O_3, and alloys were analyzed for Ni, Mn and Cu. The concentrations of Ni and Mn in the alloy samples were determined by atomic absorption spectroscopy (AAS), while Cu in the alloy was determined using sodium sulfite titration. The Cu and Ni in the slag samples were measured with AAS. The concentrations of Mn, SiO_2 and Al_2O_3 in the slag samples were measured by using ammonium ferrous sulfate titration, gravimetry and EDTA volumetric method, respectively.

3. Results and Discussion

Preliminary experiments were carried out to determine the equilibration time, and the result are shown in Fig. 2. It can be seen from Fig. 2 that a reaction time of 12 hours was sufficiently enough to achieve the equilibrium, and thus, all the experiments in this study were set to last for 12 hours. The results of this study are summarized in Table 2. Fig. 3 shows the liquidus of the "MnO"-SiO_2-Al_2O_3 system in equilibrium with Mn-Si alloy at 1623 K [28], along with the

obtained slag composition superimposed. It can be seen that both the $MnO\text{-}SiO_2$ slag and $MnO\text{-}SiO_2\text{-}Al_2O_3$ slag were near to the liquidus line at 1623 K, and saturated with silica and alumina, respectively. Some deviations can be explained by the difference of the oxygen partial pressure in this study and the data in the reported phase diagram [28].

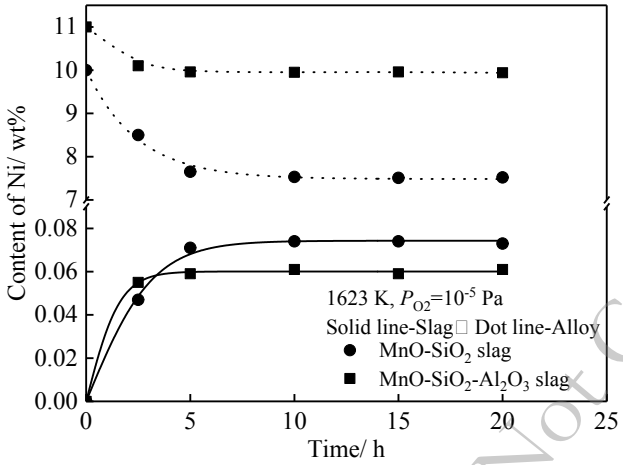

Fig. 2. Contents of nickel in slag and alloy as a function of time at 1623 K and an oxygen potential of 10^{-5} Pa.

Table 3. Analyses of equilibrated alloys and slags at 1623 K and different oxygen partial pressures

P_{O2}/ Pa	Equilibrated alloy/ wt%			Equilibrated slag/ wt%				
	Cu	Mn	Ni	Ni	Cu	MnO	SiO_2	Al_2O_3
10^{-5}	97.21	0.019	2.77	0.0300	0.65	48.64	50.51	
	94.76	0.020	5.22	0.0570	0.62	48.71	50.45	
	92.46	0.021	7.52	0.0740	0.56	47.52	51.69	
	88.47	0.024	11.51	0.0890	0.53	48.33	50.89	
10^{-6}	98.02	0.035	1.95	0.0090	0.35	47.38	52.18	
	94.33	0.041	5.63	0.0200	0.33	48.16	51.40	

	92.51	0.042	7.45	0.0240	0.33	47.92	51.64	
	91.90	0.058	8.04	0.0290	0.37	45.40	54.10	
	88.96	0.059	10.98	0.0340	0.28	48.92	50.68	
10^{-7}	97.37	0.200	2.43	0.0035	0.27	47.90	51.75	
	94.45	0.180	5.37	0.0060	0.22	47.57	52.15	
	89.22	0.190	10.59	0.0110	0.21	46.41	53.32	
	84.82	0.240	14.94	0.0130	0.19	48.58	51.17	
10^{-5}	97.63	0.050	2.32	0.0150	0.37	30.10	38.51	30.91
	97.54	0.039	2.42	0.0190	0.33	25.38	31.87	42.31
	90.00	0.040	9.96	0.0600	0.30	24.33	30.94	44.28
	86.01	0.066	13.92	0.0730	0.29	23.31	29.97	46.27
10^{-6}	96.74	0.088	3.17	0.0090	0.10	26.31	32.08	41.47
	93.07	0.096	6.83	0.0180	0.09	27.97	32.44	39.45
	89.21	0.120	10.67	0.0250	0.08	26.54	31.32	42.01
	84.55	0.170	15.28	0.0280	0.15	27.42	34.80	37.56
10^{-7}	97.37	0.200	2.43	0.0025	0.05	26.98	35.19	37.76
	94.25	0.240	5.51	0.0040	0.14	30.19	38.20	31.43
	89.98	0.250	9.77	0.0080	0.11	29.07	40.02	30.76
	85.57	0.290	14.14	0.0100	0.09	27.76	34.79	37.32

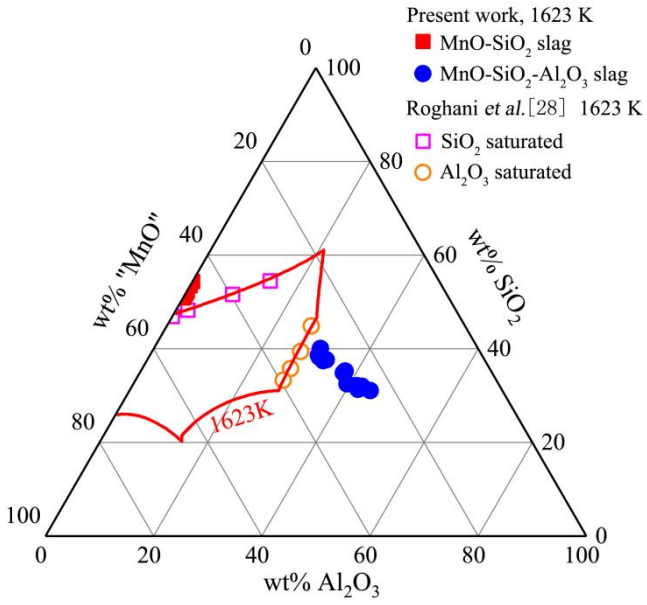

Fig. 3. Liquidus of the "MnO"-SiO_2-Al_2O_3 system in equilibrium with Mn-Si alloy at 1623 K [28], with the obtained slag composition superimposed.

3.1. The equilibrium content of NiO in slag

The contents of nickel oxide in the MnO-SiO_2 and MnO-SiO_2-Al_2O_3 slags are shown in Fig. 4, in relation to the content of Ni in equilibrated alloy phase at 1623 K and at various oxygen pressures. A general trends is observed that the content of nickel in the slag increased as the oxygen partial pressure increases. At a given oxygen partial pressure, the content of nickel oxide also increased with increasing Ni content in the alloy. It is also noted that the solubility of nickel in the MnO-SiO_2 slag was higher than that in the MnO-SiO_2-Al_2O_3 slag at same oxygen partial pressure.

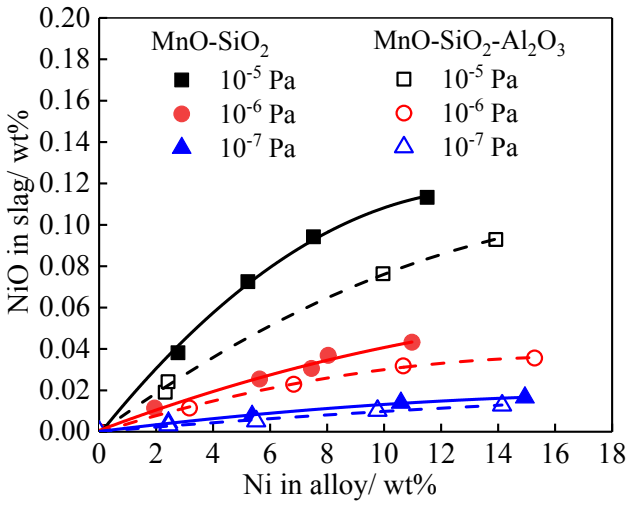

Fig. 4. Relationships between the dissolution of Ni in the $MnO\text{-}SiO_2$ and $MnO\text{-}SiO_2\text{-}Al_2O_3$ slags and the Ni content in the equilibrated alloys for at 1623 K.

Many studies have found that nickel dissolution in slag would present an amphoteric behavior based on basicity and reported nickel to dissolve in slag as Ni^{2+} in the acidic slag, while NiO_2^{2-} in the relatively basic slag [29, 30]. In this study, the mean MnO/SiO_2 for $MnO\text{-}SiO_2$ slag and $MnO\text{-}SiO_2\text{-}Al_2O_3$ slag were 0.67 and 0.92, respectively. Thus, the nickel in slag is assumed to be totally as NiO under experimental conditions. In addition, some studies have also proposed that if all the nickel in slag exist in the form of NiO, then its solubility should only be a function of the oxygen partial pressure, and will equal to 0 at $P_{O_2}^{1/2} = 0$ according to results obtained in previous studies [19, 31, 32]. In this study, the values of (wt% Ni in the slag)/a_{Ni} for $MnO\text{-}SiO_2$ slag and $MnO\text{-}SiO_2\text{-}Al_2O_3$ slag at 1623 K are plotted against the $P_{O_2}^{1/2}$ in Fig. 5. It is clear that both plots is observed to pass through the origin, thus, the nickel in both $MnO\text{-}SiO_2$ slag and $MnO\text{-}SiO_2\text{-}Al_2O_3$ slag existed as NiO under experimental conditions.

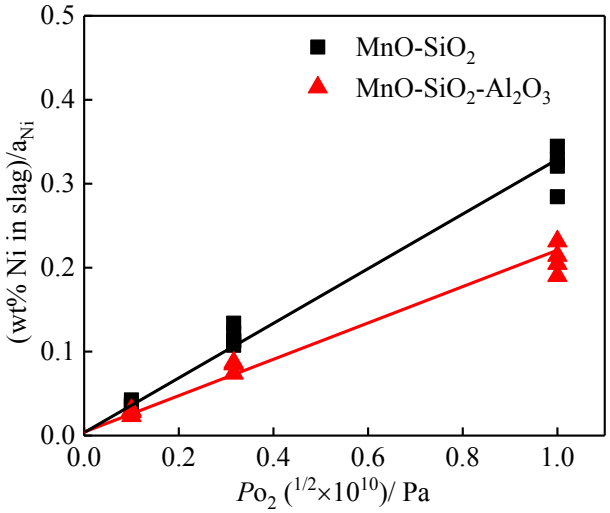

Fig. 5. Relationship between the values of (wt% Ni in slag)/a_{Ni} for MnO-SiO_2 slag or MnO-SiO_2-Al_2O_3 slag and the oxygen partial pressure at 1623 K.

3.2. Distribution ratio of Ni

The distribution ratio of Ni between the slag and alloy phases, L_{Ni}, is defined as follows:

$$L_{Ni} = \frac{x_{NiO}}{x_{Ni}} \quad (2)$$

where x_{NiO} and x_{Ni} donate the mole fractions of NiO in slag and Ni in alloy, respectively.

Fig. 6 shows the nickel distribution ratio as a function of oxygen partial pressure at 1623 K. It is clear that the nickel distribution ratio increased with increasing oxygen partial pressure, showing a linear relationship between $\log L_{Ni}$ and $\log P_{O_2}$ with a gradient of about 0.5. This can be explained by the equilibrium reaction between Ni in alloy and NiO in slag as following [23] (T/K):

$$Ni_{(l)} + 1/2O_{2(g)} = NiO_{(s)} \quad (3)$$

$$\Delta G^{\theta} = -247750 + 92.57 \times T \text{ (J/mol)} \quad (4)$$

$$\Delta G^{\theta} = -RT\ln\frac{\gamma_{NiO(s)} x_{NiO}}{\gamma_{Ni(l)} x_{Ni} (P_{O_2}/P^{\theta})^{1/2}} \quad (5)$$

where $\gamma_{NiO(s)}$ and $\gamma_{Ni(l)}$ are the activity coefficients of NiO (with respect to the pure solid NiO) and Ni (with respect to the pure liquid Ni), respectively.

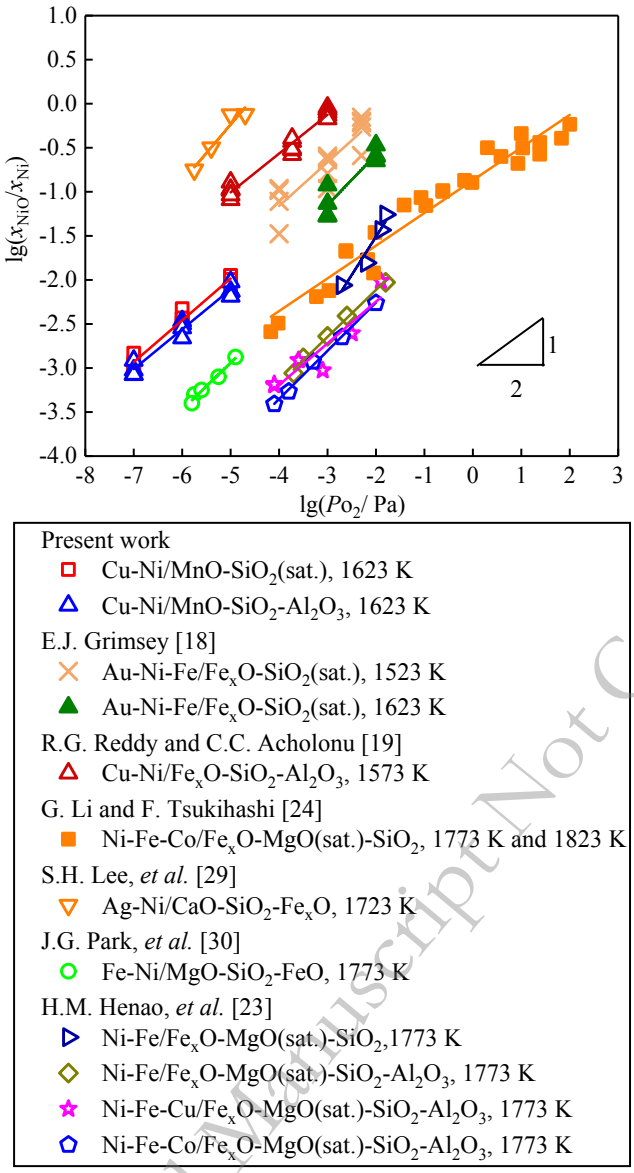

Fig. 6. Relationship of the distribution ratio of Ni against the oxygen partial pressure at 1623 K.

Thus, the logarithm of the distribution ratio of Ni can be written as following:

$$\lg L_{Ni} = \frac{1}{2}\lg P_{O_2} - \frac{1}{2}\lg P^{\theta} + \lg\left[\exp\left(-\frac{\Delta G^{\theta}}{RT}\right)\right] + \lg\frac{\gamma_{Ni}}{\gamma_{NiO}} \quad (6)$$

where ΔG^{θ} is constant at a given temperature. Therefore, if the ratios of $\gamma_{Ni(l)}$ to $\gamma_{NiO(s)}$ are constant, the $\lg L_{Ni}$ should increase in proportion to 1/2 order of the $\lg P_{O_2}$. As can be seen in Fig. 6, many works have confirmed that the ratios of $\gamma_{Ni(l)}$ to $\gamma_{NiO(s)}$ remained constant in many systems between slag and alloy, such as, Au-Ni-Fe, Ni-Fe-Co, and Cu-Ni, in equilibrium with Fe_xO-SiO_2 [18], FeO-MgO(sat.)-SiO_2 [24], and Fe_xO-SiO_2-Al_2O_3 [19] under wider temperature ranges,

respectively. Therefore, from the oxidation reaction of nickel and the distribution ratio that are expressed in Equation (6), it can be considered that the result shown in Fig. 6 is reasonable.

3.3. Activity coefficient of NiO in slag

As an important thermodynamic parameter, activity coefficient is widely used for estimating the loss of valuable metals into slag. The activity coefficient of oxide in the slag can be calculated according to Eq. (6). The activity coefficient of Ni in Cu-Ni alloy, γ_{Ni}, was calculated according to the equation (7) reported by Acholonu without considering the effect of Mn due to its low content [33].

$$\ln\gamma_{Ni} = \frac{1966}{T} x_{Cu}^2 \quad (T/\text{ K}) \tag{7}$$

Table 4. Values of activity coefficient of nickel in alloys and slags

P_{O2}/ Pa	Equilibrated alloy			Equilibrated slag			$[\gamma_{Ni}]/(\gamma_{NiO})$
	x_{Ni}	$\gamma_{Ni(l)}$	$a_{Ni(l)}$	x_{NiO}	$a_{NiO(s)}$	$\gamma_{NiO(s)}$	
$MnO\text{-}SiO_2$ slag							
10^{-5}	0.0299	3.1249	0.0935	0.00033	0.00129	3.87	0.81
	0.0563	2.9397	0.1654	0.00063	0.00227	3.60	0.82
	0.0809	2.7807	0.2250	0.00082	0.00309	3.78	0.74
	0.1234	2.5349	0.3129	0.00099	0.00430	4.36	0.58
10^{-6}	0.0211	3.1894	0.0672	0.00010	0.00029	2.94	1.09
	0.0607	2.9088	0.1765	0.00022	0.00077	3.47	0.84
	0.0802	2.7838	0.2232	0.00027	0.00097	3.66	0.76
	0.0865	2.7440	0.2373	0.00032	0.00103	3.23	0.85
	0.1178	2.5633	0.3020	0.00038	0.00131	3.49	0.74

10^{-7}	0.0263	3.1366	0.0823	0.00004	0.00011	2.93	1.07
	0.0579	2.9167	0.1688	0.00007	0.00023	3.50	0.83
	0.1136	2.5780	0.2930	0.00012	0.00040	3.32	0.78
	0.1597	2.3389	0.3736	0.00014	0.00051	3.57	0.66
$MnO-SiO_2-Al_2O_3$ slag							
10^{-5}	0.0250	3.1589	0.0789	0.00019	0.00108	5.83	0.54
	0.0260	3.1519	0.0821	0.00025	0.00113	4.56	0.69
	0.1066	2.6272	0.2800	0.00079	0.00385	4.89	0.54
	0.1485	2.4031	0.3568	0.00097	0.00491	5.08	0.47
10^{-6}	0.0341	3.0888	0.1053	0.00012	0.00046	3.92	0.79
	0.0733	2.8233	0.2068	0.00023	0.00090	3.88	0.73
	0.1141	2.5799	0.2943	0.00033	0.00128	3.93	0.66
	0.1628	2.3283	0.3790	0.00036	0.00165	4.62	0.50
10^{-7}	0.0261	3.1374	0.0820	0.00003	0.00011	3.54	0.89
	0.0591	2.9038	0.1717	0.00005	0.00024	4.75	0.61
	0.1045	2.6252	0.2744	0.00010	0.00038	3.82	0.69
	0.1507	2.3794	0.3587	0.00013	0.00049	3.87	0.61

Fig. 7 shows the activity coefficients of NiO as a function of NiO content in $MnO-SiO_2$ and $MnO-SiO_2-Al_2O_3$ slag. It is clear that the activity coefficients of NiO, referred to pure solid NiO, gradually increased as the content of NiO in the slag increased, while was independent of the oxygen partial pressure. As expected, the activity coefficient of NiO in the slag containing Al_2O_3

exhibited higher values than those in the Al_2O_3 free slag. This can be explained by considering that manganese aluminate is chemically more stable than nickel aluminate; the respective free energies of formation from the constituent oxides are -22.33 kJ for $NiO•Al_2O_3$ and -26.63 kJ for $MnO•Al_2O_3$ at 1623 K. Thus nickel oxide may be rejected from the melt in the presence of alumina, relative to manganese oxide, resulting in an increase in its activity coefficient as observed. Moreover, the relationship between activity coefficient of NiO and the content of NiO as weight percent in slag can be described by following linear equations:

γ_{NiO}=8.58(wt% NiO in slag) + 3.18 (SiO_2 saturated MnO-SiO_2 slag, 1623 K);

γ_{NiO}=11.06(wt% NiO in slag) + 4.07 (Al_2O_3 saturated MnO-SiO_2-Al_2O_3 slag, 1623 K).

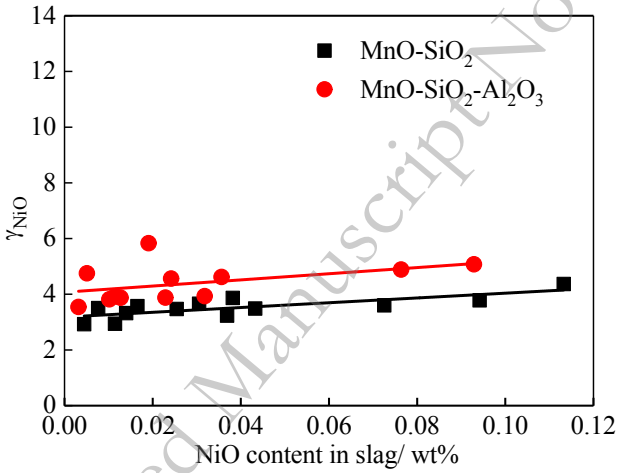

Fig. 7. Activity coefficient of nickel oxide relative to pure solid nickel oxide vs wt% nickel oxide in different slag systems at 1623 K.

As mentioned above, the alumina is a welcome addition in MnO-SiO_2 slag for the smelting reduction of the polymetallic sea nodules, since the higher activity coefficient of NiO, the lower losses to the slag. Considering the plenty of metallic Al in the spent LIBs, the reduction smelting of polymetallic sea nodules could be optimized by adding the spent LIBs, producing a MnO-SiO_2-Al_2O_3 slag rather than MnO-SiO_2 slag.

4. Conclusions

As a fundamental study related to the smelting-reduction of both spent lithium-ion batteries and polymetallic sea nodules, experiments were conducted by the phase equilibrium between Cu-Ni alloy and SiO_2 saturated $MnO\text{-}SiO_2$ or Al_2O_3 saturated $MnO\text{-}SiO_2\text{-}Al_2O_3$ slags under controlled oxygen partial pressure of 10^{-7}, 10^{-6}, and 10^{-5} Pa at 1623 K. The results show that the distribution ratios of Ni and the solubility of nickel oxide in the slag increased with increasing oxygen partial pressure. The addition of Al_2O_3 in the $MnO\text{-}SiO_2$ slag decreased the dissolution of Ni in the slag, and increased the activity coefficient of NiO. Furthermore, the activity coefficient of NiO referred to the pure solid NiO can be calculated as:

γ_{NiO}=8.58(wt% NiO in slag) + 3.18 (SiO_2 saturated $MnO\text{-}SiO_2$ slag, 1623 K);

γ_{NiO}=11.06(wt% NiO in slag) + 4.07 (Al_2O_3 saturated $MnO\text{-}SiO_2\text{-}Al_2O_3$ slag, 1623 K).

Acknowledgements

This work was supported by the National Natural Science Foundation of China (Grant No. 51704038).

References

1. C. Hanisch, J. Diekmann, A. Stieger, W. Haselrieder, and A. Kwade, *Recycling of Lithium-Ion Batteries, Handbook of Clean Energy Systems*, John Wiley & Sons, Ltd., Chichester, 2015, p. 1.

2. A. Home, LME stock surge grounds high-flying nickel, but for how long?, https://www.mining.com/web/lme-stock-surge-grounds-high-flying-nickel-but-for-how-long/

3. Electric vehicle growth creates East-Asian battery mineral boom,

https://www.prnewswire.com/news-releases/electric-vehicle-growth-creates-east-asian-battery-mineral-boom-301014990.html

4. M. Chen, X. Ma, B. Chen, R. Arsenault, P. Karlson, N. Simon, and Y. Wang, Recycling end-of-life electric vehicle lithium-ion batteries, *Joule*, 3(2019), p. 1.

5. R. Guoxing, X. Songwen, X. Meiqiu, P. Bing, F. Yougi, W. Fenggang, and X. Xing, Recovery of valuable metals from spent lithium-ion batteries by smelting reduction process based on $MnO\text{-}SiO_2\text{-}Al_2O_3$ slag system, [in] *Advances in Molten Slags, Fluxes, and Salts: Proceedings of the 10th International Conference on Molten Slags, Fluxes and Salts*, Seattle, 2016, p. 211.

6. P.K. Sen, Metals and materials from deep sea nodules: an outlook for the future, *Int. Mater. Rev.*, 55(2010), No. 6, p. 364.

7. G. Senanayake, Acid leaching of metals from deep-sea manganese nodules-a critical review of fundamentals and applications, *Miner. Eng.*, 24(2011), p. 1379.

8. N.S. Randhawa, J. Hait, and R.K. Jana, A brief overview on manganese nodules processing signifying the detail in the Indian context highlighting the international scenario, *Hydrometallurgy*, 165(2016), p. 166.

9. E.H. Jeong, C.W. Nam, K.H. Park, and J.H. Park, Sulfurization of Fe-Ni-Cu-Co alloy to matte phase by carbothermic reduction of calcium sulfate, *Metall. Mater. Trans. B*, 47B(2016), p. 1103.

10. S. Agarwal, K.K. Sahu, R.K. Jana, and S.P. Mehrotra, Recovery of Cu, Ni, Co and Mn from sea nodules by direct reduction smelting, [in] *Proceedings of The Eighth (2009) ISOPE Ocean Mining Symposium*, Chennai, 2009, p. 131.

11. D. Friedmann, A.K. Pophanken, and B. Friedrich, Pyrometallurgical treatment of high manganese containing deep sea nodules, *J. Sustain. Metall.*, 3(2017), p. 219.

12. K.D. Mehta, C. Das, and B.D. Pandey, Leaching of copper, nickel and cobalt from Indian ocean manganese nodules by aspergillus niger, *Hydrometallurgy*, 105(2010), p. 89.

13. R. Barik, K. Sanjay, B.K. Mishra, and M. Mohapatra, Micellar mediated selective leaching of manganese nodule in high temperature sulfuric acid medium, *Hydrometallurgy*, 165(2016), p. 44.

14. S.C. Das, Extraction of metals from polymetallic ocean nodules, [in] *Proceeding national symposium on chemical and allied materials from ocean*, Calcutta, 1989, p. 9.

15. S. Xiao, G. Ren, M. Xie, B. Pan, Y. Fan, F. Wang, and X. Xia, Recovery of valuable metals from spent lithium-ion batteries by smelting reduction process based on MnO-SiO_2-Al_2O_3 slag system, *J. Sustain. Metall.*, 3(2017), No. 4, p. 703.

16. N.S. Randhawa, R.K. Jana, and N.N. Das, Silicomanganese production utilising low grade manganese nodules leaching residue, *Miner. Process. Ext. Metall. (Trans. IMM-C)*, 122(2013), p. 6.

17. M. Sommerfeld, D. Friedmann, T. Kuhn, and B. Friedrich, "Zero-waste": a sustainable approach on pyrometallurgical processing of manganese nodule slags, *Minerals*, 8(2018), p. 544.

18. E.J. Grimsey, The effect of temperature on nickel solubility in silica saturated fayalite slags from 1523 to 1623 K, *Metall. Trans. B*, 19B(1988), p. 243.

19. R.G. Reddy and C.C. Acholonu, Distribution of nickel between copper-nickel and alumina saturated iron silicate slags, *Metall. Trans. B*, 15B(1984), p. 33.

20. H.M. Henao, M. Hino, and K. Itagaki, Equilibrium between Ni-S melt and FeO_x-SiO_2 or FeO_x-CaO based slag under controlled partial pressures, *Mater. Trans.*, 43(2002), No. 9, p. 2219.

21. Y. Takeda, S. Ishiwata, and A. Yazawa, Distribution equilibria of minor elements between liquid copper and calcium ferrite slag, *Trans. Jpn. Inst. Met.*, 24(1983), No. 7, p. 518.

22. R.U. Pagador, M. Hino, and K. Itagaki, Distribution of minor elements between MgO saturated FeO_x-MgO-SiO_2 or FeO_x-CaO-MgO-SiO_2 slag and nickel alloy, *Mater. Trans., JIM*, 40(1999), No. 3, p. 225.

23. H.M. Henao, M. Hino, and K. Itagaki, Distribution of Ni Cr Mn Co and Cu between Fe-Ni alloy and FeO-MgO-SiO_2 base slags, *Mater. Trans.*, 42(2001), No. 9, p. 1959.

24. G.Q. Li and F. Tsukihashi, Distribution equilibria of Fe, Co and Ni between MgO-saturated FeO_x-MgO-SiO_2 slag and Ni alloy, *ISIJ Int.*, 41(2001), No. 11, p. 1303.

25. H.M. Henao, M. Hino, and K. Itagaki, Phase equilibrium between Ni-S melt and CaO-Al_2O_3 based slag in CO-CO_2-SO_2 gas mixtures at 1773 K, *Mater. Trans.*, 43(2002), No. 11, p. 2873.

26. H.M. Henao and K. Itagaki, Phase equilibrium and distribution of minor elements between Ni-S melt and Al_2O_3-CaO-MgO slag at 1873 K, *Metall. Mater. Trans. B*, 35B (2004), p. 1041.

27. X. Lu, T. Miki, and T. Nagasaka, Activity coefficients of NiO and CoO in CaO-Al_2O_3-SiO_2 slag and their application to the recycling of Ni-Co-Fe-based end-of-life superalloys via remelting, *Int. J. Miner. Metall. Mater.*, 24(2017), No. 1, p. 25.

28. G. Roghani, E. Jak, and P. Hayes, Phase Equilibrium Studies in the "MnO"-Al_2O_3-SiO_2 System, *Metall. Mater. Trans. B*, 33B (2002), p. 827.

29. S.H. Lee, S.M. Moon, J.H. Park and D.J. Min, Thermodynamic behavior of nickel in CaO-SiO_2-Fe_tO slag, *Metall. Mater. Trans. B*, 33B(2002), p. 55.

30. J.G. Park, H.S. Eom, W.W. Huh, Y.S. Lee, D.J. Min, and I. Sohn, A study in the thermodynamic behavior of nickel in the MgO-SiO_2-FeO slag system, *Steel Research Int.*, 82(2011), No. 4, p. 415.

31. E.J. Grimsey and X.L. Liu, The activity coefficient of cobalt oxide in silica-saturated iron

silicate slags, *Metall. Mater. Trans. B*, 26B(1995), p. 229.

32. B. Derin and O. Yücel, The distribution of cobalt between Co-Cu alloys and Al_2O_3-FeO-Fe_2O_3-SiO_2 slags, *Scand. J. Metall.*, 31(2002), No. 1, p. 12.

33. C. Acholonu, *Distribution of copper, cobalt, nickel, between alloys and silica-unsaturated iron slags* [Dissertation], University of Nevada, Reno, 1983, p. 9.